Hindawi Publishing Corporation
Journal of Nanomaterials
Volume 2016, Article ID 9747931, 12 pages
http://dx.doi.org/10.1155/2016/9747931

Research Article

The Roll of NaPSS Surfactant on the Ceria Nanoparticles Embedding in Polypyrrole Films

Simona Popescu, Mihaela Mîndroiu, Daniela Cabuzu, and Cristian Pîrvu

University Politehnica of Bucharest, 313 Splaiul Independentei, Sector 6, 060042 Bucharest, Romania

Correspondence should be addressed to Cristian Pîrvu; c_pirvu@chim.upb.ro

Received 27 October 2015; Revised 8 April 2016; Accepted 14 April 2016

Academic Editor: Paulo Cesar Morais

Cerium oxide nanoparticles (CeO_2 NPs) in crystalline form have been synthesized by a coprecipitation method. CeO_2 nanoparticles were then embedded in polypyrrole (PPy) films during the electropolymerization of pyrrole (Py) on titanium substrate. The influence of poly(sodium 4-styrenesulfonate) (NaPSS) surfactant used during polymerization on the embedding of CeO_2 NPs in polypyrrole films was investigated. The new films were characterized in terms of surface analysis, wettability, electrochemical behaviour, and antibacterial effect. The surface and electrochemical characterization revealed the role of surfactant on PPy doping process cerium oxide incorporation. In the presence of surfactant, CeO_2 NPs are preferentially embedded in the polymeric film while, without surfactant, the ceria nanoparticles are quasiuniformly spread as agglomerates onto polymeric films. The antibacterial effect of studied PPy films was substantially improved in the presence of cerium oxide and depends by the polymerization conditions.

1. Introduction

Nowadays, titanium still represents a solution for the choice of base-implant materials in orthopedic and dental field, due to its excellent properties that refers to corrosion resistance and mechanical properties. Many studies have confirmed the necessity of titanium implants pretreatments, in order to accelerate the process of its integration within the surrounding tissue, by designing a new titanium-based material with a bioactive surface [1–5]. The novelty in this domain came always from the ingenuity of methods that have developed in a dynamic way.

Among the variety of methods used to modify the titanium surface in a "friendly" way, the deposition of an adherent, biocompatible, polymer film on titanium represents a simple and efficient alternative [6–10]. In this way, the reactivity of polymer surface could be further implied in the process of biologically active molecules grafting [11, 12]. Another advantage is related to protection of the metal against corrosion and avoiding the problem of ions release in the surrounding tissue [13, 14]. Moreover, these polymers have the doping ability with different molecules, during their polymerization, thus improving the surface properties for appropriate application [15–17]. The choice of polypyrrole (PPy) as conducting polymer for metallic substrate coating is based on its simple electrochemical polymerization directly onto metallic substrates [18, 19]. Other important properties, such as high electronic conductivity, good stability regarding the resistance against corrosion in aqueous solution, and good biocompatibility with respect to several cells types *in vitro* and *in vivo,* were also highlighted in literature [20–23].

Besides aspects related to biocompatibility, a major importance was focused on antibacterial activity, since the ever-increasing resistance of pathogens towards antibiotics represents major postimplantation problems. Bacteria are able to adapt rapidly to new unfavorable environmental conditions; hence, their resistance to antimicrobial molecules increased substantially. Considering this issues, in the last years the metal oxide nanoparticles have gained attention in developing of new drug delivery systems and antibacterial agents [24–26]. Metal oxide NPs are an important class of inorganic compounds due to their special properties in different domains: optical, magnetic, electronic properties and medicine. Among them, cerium oxide (CeO_2) became more

and more utilized as antioxidant, providing an efficient protection against free radicals and as antimicrobial agent [27–29]. The small size of particles allows the interaction with biological entities (proteins, DNA molecules, and membranes).

In this respect, as a polymeric matrix, PPy has been already subjected to incorporation of different antibacterial substances such as silver nanoparticles [30, 31] biodegradable compounds such as dextrin or chitosan [32, 33], PEG [34], or other carotenoid compounds like torularhodin [35].

The idea of combining a polymer with nanoparticles to create a composite material represents a promising alternative since these materials combine both the unique properties of nanoparticles with those of the polymer, resulting in a new material with specific properties. The incorporation of ceria particles in polypyrrole film requires some special precautions. These particles are stabilized by electrostatics forces and are extremely sensitive to perturbations of pH, ionic strength, and concentration that may dramatically modify their thermodynamic stability. The low stability occurs due to high surface-to-volume ratio for particles and from the strong reactivity of the surface chemical sites to physicochemical changes. Therefore, for some applications, the challenge is to find appropriate conditions to prepare CeO_2 polymeric composite in which ceria nanoparticles are dispersed homogeneously in a polymer matrix [36].

Literature contains one study about the incorporation of CeO_2 in dodecyl sulfate doped polypyrrole films (PPy-DS) deposited on gold electrode. It was concluded that CeO_2 NPs have the ability to modify the morphology of electrodeposited PPy-DS thin films, but without highlighting the film morphology and the influence of the surfactant on ceria nanoparticles distribution into the polymeric film [37].

In the present study, poly(sodium 4-styrenesulfonate) (NaPSS) was selected as surfactant based on previous studies [38, 39] and it is expected to provide a good CeO_2 distribution and a better embedding in the polymer nanocomposite film deposited on titanium surface. Two PPy-CeO_2 composite films obtained with and without NaPSS were studied comparatively, in terms of surface properties, electrochemical stability, and antibacterial activity.

2. Experimental Part

2.1. Synthesis of CeO_2 Nanoparticles. For the synthesis of CeO_2 nanoparticles we applied a simple hydroxide mediated approach that uses cerium nitrate hexahydrate ($Ce(NO_3)_3{\cdot}6H_2O > 99.5\%$; Aldrich Chemicals, USA) as starting material and sodium hydroxide as precipitating agent. All the chemical reagents were used without purification.

The starting solutions were 0.1 M $Ce(NO_3)_3{\cdot}6H_2O$ and 0.3 M NaOH, prepared with double distilled water. First step consists in adding dropwise the NaOH solution for 3 hours, under continuous stirring at room temperature until a pinkish precipitate is obtained. The vigorous stirring is very important because it influences the product particle size and its distribution.

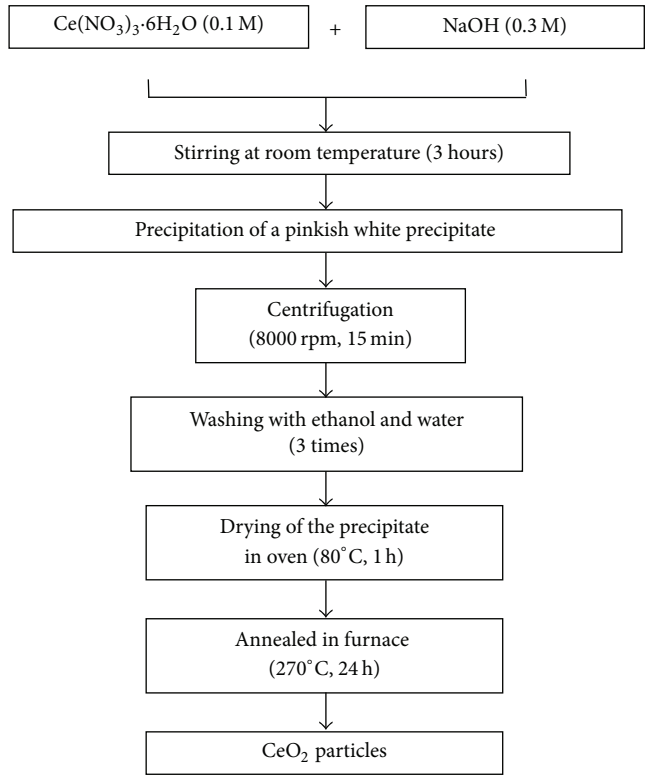

Figure 1: Synthesis of CeO_2 nanoparticles.

The apparition of a pinkish precipitate suggests the oxidation of $Ce(OH)_3$ into $Ce(OH)_4$ that occurs in the presence of dissolved oxygen, while the pH was maintained around 9. Finally, it became a light yellow suspension, characteristic for CeO_2.

The reactions during the synthesis are the following:

$$Ce\left(NO_3\right)_3 \cdot 6H_2O_{(s)} \longrightarrow Ce^{3+}_{(aq)} + 3NO^{-}_{3(aq)} + 6H_2O \quad (1)$$

$$2Ce^{3+}_{(aq)} + \frac{1}{2}O_2 + 6OH^{-} \xrightarrow{pH\approx 9} 2CeO_2 + 3H_2O \quad (2)$$

In another step, the yellow precipitate was centrifuged three times, washed well with ethanol and distilled H_2O three times, and then dried in an oven at 80°C for 1 hour, followed by an annealing process at 270°C for 24 h. The resulting precipitate is a light yellow precipitate that was further analyzed through XRD. Figure 1 presents the schematic diagram for CeO_2 particles synthesis.

2.2. Preparation of Titanium Substrate before Polymer Films Electrodeposition. Commercially pure Ti discs of 10 mm diameter and 1 mm thickness (99.6% purity, grade 2, Goodfellow Cambridge Ltd., UK) were used. The surface of test specimens was polished with SiC paper to grade 4000 and then washed with a large amount of water followed by acetone and finally rinsed with distilled water and dried in air at room temperature.

2.3. Synthesis of PPy Films and PPy-CeO_2 with and without Surfactant. Synthesis of polymeric films was performed by

potentiodynamic polymerization method. Polypyrrole films were electrodeposited on titanium substrate (Ti/PPy) from an aqueous solution containing freshly distilled pyrrole (Py 0.4 mol·dm^{-3} purchased from Merck, purity > 98%) and oxalic acid (0.2 mol·dm^{-3}) as support electrolyte. Nanocomposite films were obtained by adding cerium oxide nanoparticles (CeO_2 NPs, 40 μg·mL^{-1}) in the electrolytic solution (Ti/PPy-CeO_2 NPs). CeO_2 NPs were ultrasonically dispersed prior to the proper electrosynthesis step. In order to modify the surface characteristics of the polymer films, NaPSS (0.1 mol·dm^{-3}) was added in the polymerization solution (Ti/PPy-NaPSS). The optimal surfactant concentration was established in a previous work [38]. The surfactant was also introduced along with CeO_2 NPs in the composition of polymerization solution to study its influence on nanoparticles incorporation in the polymeric films (Ti/PPy-NaPSS-CeO_2 NPs). All solutions were prepared using ultra-pure deionized Milli-Q water.

The films electrosynthesis was carried out using one compartment cell with three electrodes: titanium as working electrode, platinum counter electrode and Ag/AgCl, and KCl reference electrode, connected to an Autolab PGSTAT 302N potentiostat with general-purpose electrochemical system software. Polymerization was performed by applying 5 consecutive cyclic voltammetric scans between 0 and 0.95 V versus Ag/AgCl using a 50 mV·s^{-1} scan rate.

2.4. Methods for Polymer Nanocomposite Coatings Characterization

2.4.1. Surface Characterization. Scanning electron microscopy (SEM) images were taking with FEI Nova NanoSEM 630 FEG-SEM (SEM with Field Emission Gun) with ultra-high resolution characterization at high and low voltage in high vacuum. The voltage of SEM analysis was 20 kV and the magnification of the images was between 1000x and 50000x. The elemental composition was investigated using Carl Zeiss Evo 50 XVP scanning electron microscope (SEM) equipped with energy dispersive X-ray analysis (EDAX) Quantax Bruker 200 accessory.

X-ray diffraction (XRD): the crystalline nature of CeO_2 particles was analyzed using a Rigaku Ultima IV X-ray diffractometer in Bragg Brentano parafocusing setup with high resolution, using CuKα radiation (λ = 0.154 nm). The source was operated at 40 kV and 40 mA.

The contact angle of a drop of water with the films surface was measured with a Contact Angle Meter-KSV Instruments CAM 100 equipment. The hydrophilic/hydrophobic balance of synthesized films was evaluated by measuring the static contact angle (θ) of a drop of water deposited on the studied film surface. Each contact angle value is the mean value from 5 measurements. The investigation was carried out at 25°C.

2.4.2. Electrochemical Characterization. Electrochemical stability evaluation was performed at room temperature, using potentiostatic assembly with a single compartment and three electrodes: *working electrode* (samples Ti, Ti/PPy, Ti/PPy-CeO_2 NPs, Ti/PPy-NaPSS, and Ti/PPy-NaPSS-CeO_2 NPs), a *counter electrode* (Metrohm Pt disk), and *a reference electrode* (Metrohm Ag/AgCl, 3 M KCl) connected to an Autolab PGSTAT 302N potentiostat/galvanostat. The data were collected with NOVA 1.10 software.

All electrochemical characterizations were made in an aqueous buffer testing solution composed of NaCl 8.74 g·L^{-1}, $NaHCO_3$ 0.35 g·L^{-1}, $Na_2HPO_4{\cdot}12H_2O$ 0.06 g·L^{-1}, and NaH_2PO_4 0.06 g·L^{-1} at pH 6.7. The substances were purchased from Sigma-Aldrich Corp. (St. Louis, MO, USA).

Polarization curves were registered at ±200 mV versus OCP, at a scan rate of 2 mV/s and corrosion parameters were computed based on Tafel plots: i_{cor} (corrosion current density), R_p (polarization resistance), E_{cor} (corrosion potential), and v_{cor} (corrosion rate). For electrochemical experiments the electrode area exposed to the solution was 0.2826 cm^2.

Cyclic potentiodynamic polarization was performed starting from −0.5 V to 0.5 V, with a scan rate of 100 mV/s, 10 cycles in buffer solution.

The *electrochemical impedance spectra* (EIS) were acquired in the frequency range of 0.1–10^5 Hz in order to obtain Nyquist plots by applying a small excitation amplitude of 10 mV.

The *Mott-Schottky* measurements were made from a start potential of −0.5 V to an end potential of 0.5 V with a step potential of 0.05 V. In this work, a frequency of 10 kHz for Mott-Schottky measurements was applied [40].

2.4.3. Antibacterial Activity Evaluation of Polymer Nanocomposite Coatings. The antibacterial activity of polymer nanocomposite films was tested against human pathogenic microbial strain, *Escherichia coli* ATCC 8738. The bacterial strains were grown in Luria Bertani Agar (LBA) plates at 37°C with the following composition: peptone (Merck), 10 g·L^{-1}; yeast extract (Biolife) 5 g·L^{-1}, NaCl (Sigma-Aldrich) 5 g·L^{-1}, and agar (Fluka) 20 g·L^{-1}.

The stock culture was maintained at 4°C. All aqueous solutions were prepared with deionized water. To exploit antibacterial potential of the samples Kirby-Bauer disk-diffusion method was performed [41]. In brief, sterile LBA plates were prepared by pouring the sterilized media in sterile Petri plates under aseptic conditions. The bacterial strain, 1 mL, was spread on agar plates and then sterile samples were applied on plate surface. At the end of the incubation time (24 h), the diameter of microbial growth inhibition halo was measured in millimeters [35].

3. Results and Discussion

3.1. Characterization of CeO_2 Nanoparticles Powder

3.1.1. XRD Characterization. The crystalline nature of CeO_2 nanoparticles prepared according to hydroxide mediated approach can be deduced from the X-ray diffraction spectra shown in Figure 2. The XRD pattern of the heat treated powder was registered from 10 to 90 degrees, $2\theta/\theta$ scan axis, with 0.02° angular step and 0.5 sec/step. The resulting pattern revealed the formation of well-crystallized single phase material. The chemical synthesized powder exhibits lines that

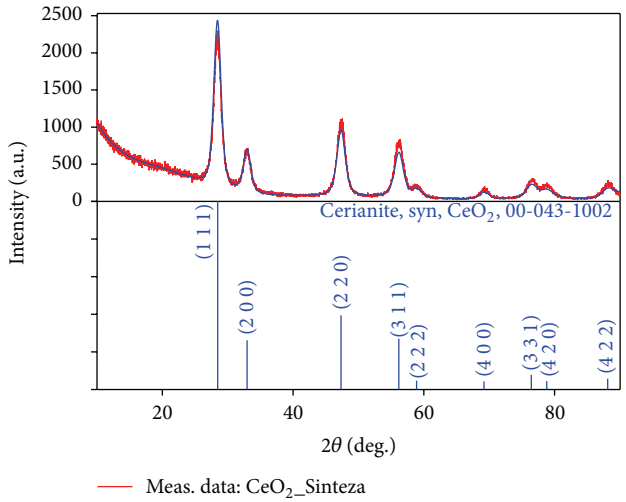

FIGURE 2: XRD diffraction patterns of ceria nanoparticles (CeO_2).

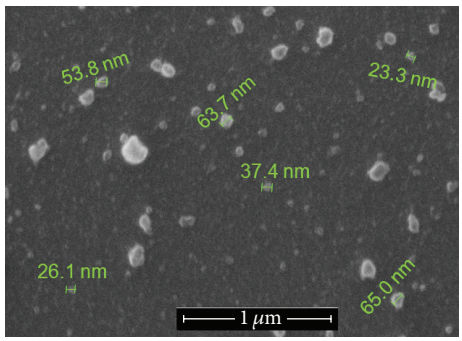

FIGURE 3: SEM image obtained on CeO_2 powder prepared by hydroxide mediated approach.

correspond to crystal planes (111), (200), (220), (311), (222), (400), (331), (420), and (422) that are characteristics for CeO_2, according to those of centered face cubic (CFC) fluorite structured CeO_2 crystal. No extra peaks corresponding to any other secondary phases are observed.

The crystal planes were in accordance with ICDD (PDF2.DAT) (CeO_2/Cerianite, syn, DB card number 00-043-1002). The diffraction peaks in these XRD spectra indicate the pure cubic fluorite structure.

3.1.2. SEM Characterization. SEM images of CeO_2 powder prepared by hydroxide mediated approach are shown in Figure 3. From the SEM images, it was found that CeO_2 particles are characterized by a size of the powder in the range 20–70 nm. Also, there were some visible aggregates formed by particles quite agglomerated.

3.2. Electrosynthesis of Polypyrrole Nanocomposite Thin Films on Titanium Electrodes. The CV curves from electrodeposition of PPy films on titanium substrate are presented in Figure 4.

For all samples the current density gradually increases in the successive CV cycles, showing the electrodeposition

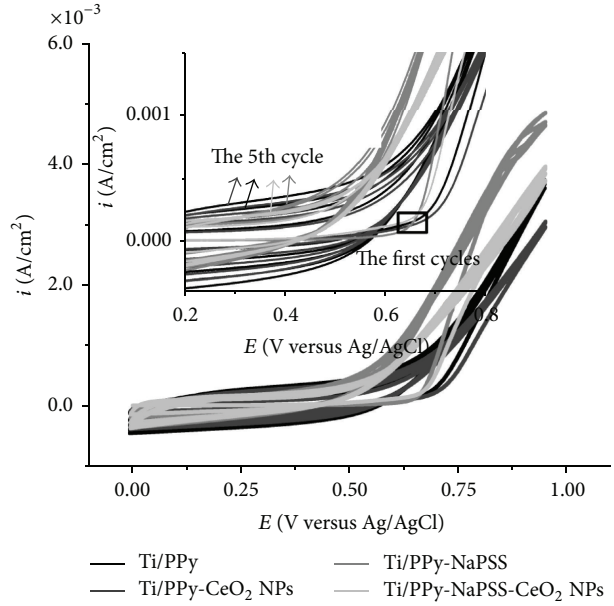

FIGURE 4: Cyclic voltammograms of PPy-nanocomposite films electrodeposition on titanium substrate.

of polypyrrole or polypyrrole nanocomposite films onto titanium substrate.

The presence of NaPSS surfactant in the polymerization solution seems to improve Py polymerization rate. The total electric charge used for polymerization is higher in the presence of NaPSS (0.40 C/cm^2) comparing to PPy film (0.24 C/cm^2), as can be seen from Figure 5. If we consider that the entire charge is used for polymerization process, this can be an indication that the thickness of the polymer film obtained in the presence of surfactant is higher. During the polymerization of pyrrole, PSS^- has three different roles: PSS^- (i) stabilizes the radical cation of the pyrrole monomer, (ii) acts as a charge balancing dopant for PPy, and (iii) renders the dispersion of the growing PPy chains in the final polymer film. Small oxalate molecule dopants have a similar doping function; however they did not render the final complex dispersible [42].

By adding CeO_2 NPs in polymerization solution that contains pyrrole monomer and oxalic acid (pH = 1.4), the total charge used for polymerization decreases to 0.20 C/cm^2. In this pH conditions the ceria nanoparticles are positively charged, according to literature [43]. Py^+ cationic radical stability in the polymerization process was diminished, and thus the electrodeposition rate decreased. Electrostatic repulsions between positive cerium oxide and PPy^+ could result in pushing positive CeO_2 nanoparticles to the surface of polymer film during polymerization, Figure 6(a).

Different behaviour can be observed when CeO_2 NPs are added in the pyrrole and NaPSS acid polymerization solution. In the presence of surfactant the surface charge of CeO_2 NPs became negative as a consequence of adsorption of PSS^- anions on their surface [43]. Thus, due to the electrostatic interactions between, in this situation, negatively charged CeO_2 nanoparticles and cationic PPy^+ matrix (doping) the

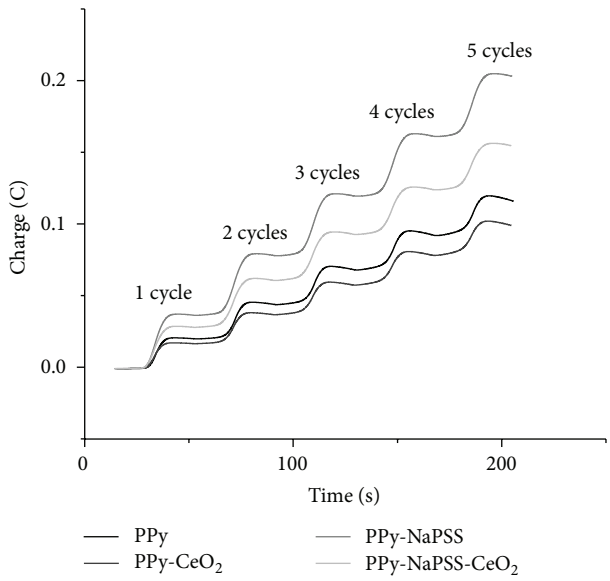

Figure 5: Electrical charge evolution with polymerization time for polymer nanocomposite films.

compacting degree of the polymeric film is expected to be improved, Figure 6(b). In this case the total electrical charge used for polymerization decreases from 0.40 C/cm^2 to 0.32 C/cm^2. The embedding of CeO_2 NPs in PPy matrix starts right from the first cycle when the titanium surface is positively charged by the decrease of the Fermi level due to electrode anodic polarization. Moreover, the negatively charged ceria nanoparticle and PSS^- could be directly adsorbed on the positively charged titanium surface.

These different interactions between PPy^+ and positively/negatively charged CeO_2 NPs are intended to bring major changes in terms of morphology, wettability, electrochemical stability, and antibacterial activity of these polymer nanocomposite films.

3.3. Surface Characterization of PPy-Nanocomposite Films

3.3.1. SEM and EDAX Analysis. The SEM images corresponding to surface of PPy-CeO_2 NPs and PPy-NaPSS-CeO_2 NPs are illustrated in Figure 7. The surface morphology analysis sustains and completes the expected changes in the polymeric films structure, due to the role played by the surfactant on CeO_2 NPs embedded in PPy films.

Figure 7(a) reveals a quasiuniform spreading of CeO_2 NPs agglomerates onto polymeric matrix. This confirms the presumed idea, from anterior section, sustaining the nanoparticles pushed from the inside to outside polymer film surface, due to the electrostatic repulsion between positively charged CeO_2 NPs and PPy^+ as was represented in Figure 6(a). CeO_2 NPs agglomeration can be associated with (i) suggested electrostatic repulsions towards PPy^+, (ii) low stability occurred due to high surface-to-volume ratio, and (iii) strong reactivity of the nanoparticles surface chemical sites. From Figure 7(b) both CeO_2 NPs aggregates of hundreds nanometers and free nanoparticles with dimension less than 50 nm can be observed.

Table 1: EDAX analyzes for PPy film, PPy-CeO_2 NPs film, and PPy-NaPSS-CeO_2 NPs film.

Samples	Element					
	Ti	C	N	O	Ce	S
	(Atomic%)					
Ti/PPy	50.77	21.55	9.72	15.94	—	—
Ti/PPy-CeO_2 NPs	35.97	33.5	10.64	19.16	0.33	—
Ti/PPy-NaPSS-CeO_2 NPs	24.07	42.32	11.4	20.42	0.32	1.28

Comparatively, in Figure 7(c), the surface morphology of PPy-NaPSS-CeO_2 NPs is presented. CeO_2 NPs aggregates are less numerous than on PPy-CeO_2 NPs surface and their sizes are also more reduced. The small amount of CeO_2 NPs aggregates on the surface could be an additional argument to the fact that, in the presence of surfactant, negatively charged CeO_2 NPs are preferentially embedded in the polymeric film due to the electrostatic interactions with PPy^+ (doping process) mentioned above. Figure 7(d) shows CeO_2 NPs aggregates with dimensions comprised between 150 nm and 300 nm and the amount of nonassociated nanoparticles between 50 nm and 80 nm seems to be greater.

Moreover, the most important information highlighted by EDAX analysis consists in proving of CeO_2 NPs presence on/into the polymer film. Furthermore, the cerium amount is almost the same, about 0.32 at %, for both PPy-CeO_2 NPs and PPy-NaPSS-CeO_2 NPs film (Table 1). This means that almost the same quantity of CeO_2 NPs is differently distributed: mainly on PPy surface for PPy-CeO_2 NPs film and preferentially into polymer matrix for PPy-NaPSS-CeO_2 NPs film, as was concluded from electrochemical deposition and SEM analyses.

The increasing in atomic% for C and N elements (provided by polypyrrole) for PPy-CeO_2 NPs comparing with PPy indicates a higher amount of polypyrrole. However, the corresponding electrical charge used for polymerization was diminished (from 0.24 C/cm^2 to 0.20 C/cm^2, Figure 5), suggesting a negative influence of CeO_2NPs over PPy doping process. In the presence of NaPSS and CeO_2 NPs (PPy-NaPSS-CeO_2 NPs) the amount of PPy (suggested by an increasing in atomic% of C and N) sustains the presumption mentioned in Section 3.2, according to which the thickness of the polymer film obtained in the presence of surfactant is higher.

3.3.2. Surface Wettability. The surface wettability is an important feature for many applications that implies the surface interaction with different biological entities such as bacteria or cells.

The contact angle measurements of the studied surfaces are presented in Table 2.

PPy film has a low hydrophobic behaviour. The presence of CeO_2 NPs on the polymeric film (PPy-CeO_2 NPs) leads to a decrease of the contact angle from 86.61° to 78.64°.

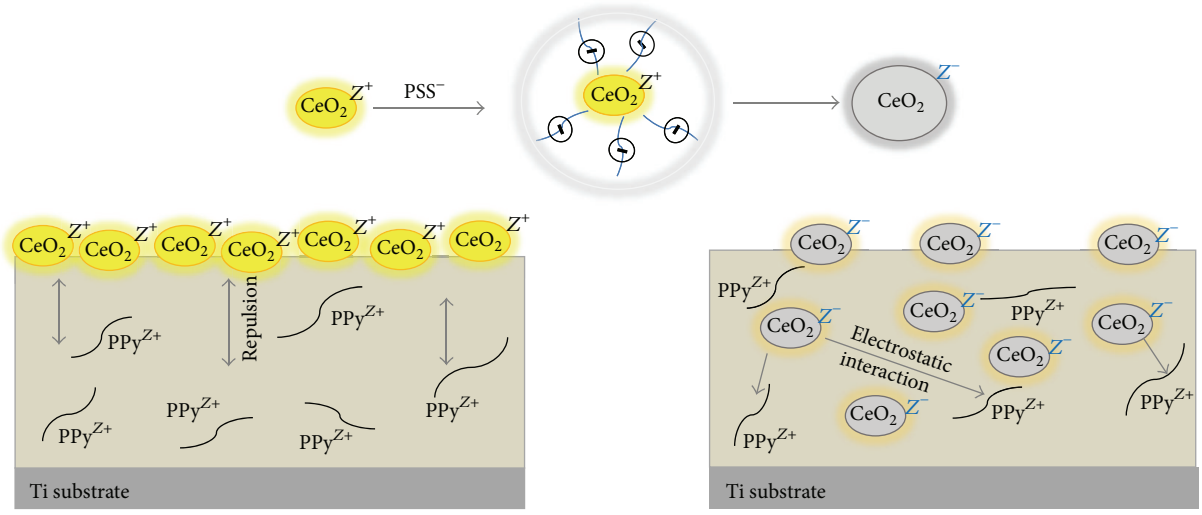

FIGURE 6: Electrostatic repulsions between positive cerium oxide and PPy^+ (a); electrostatic interactions between negatively charged CeO_2 nanoparticles (in the presence of NaPSS) and cationic PPy^+ matrix (b).

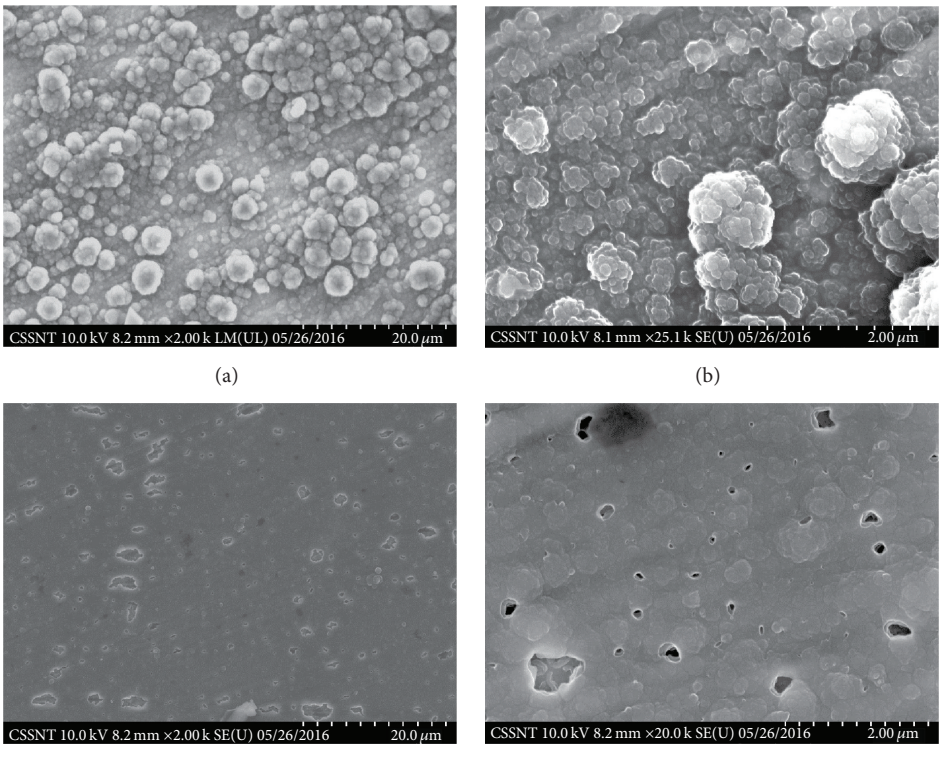

FIGURE 7: SEM images for PPy-CeO_2 NPs ((a) and (b)) and PPy-NaPSS-CeO_2 NPs ((c) and (d)) nanocomposite films, electrodeposited from electrolytic aqueous solution containing pyrrole (0.4 mol·dm^{-3}), CeO_2 NPs (40 μg·mL^{-1}), and NaPSS (0.1 mol·dm^{-3}).

However, the hydrophilic property of polymeric film was increased when the polymerization was performed in the presence of NaPSS surfactant. The contact angles for films in which NaPSS is present (Ti/PPy-NaPSS and Ti/PPy-NaPSS-CeO_2 NPs) are very close (52.15° and 53.88°). This can be explained by the less influence of CeO_2 NPs on the wettability of the polymer film due to its embedding in the polymer matrix. Moreover, the effect of CeO_2 NPs bonded at the surface upon wettability is insignificant due to adsorption of NaPSS molecules on ceria nanoparticles.

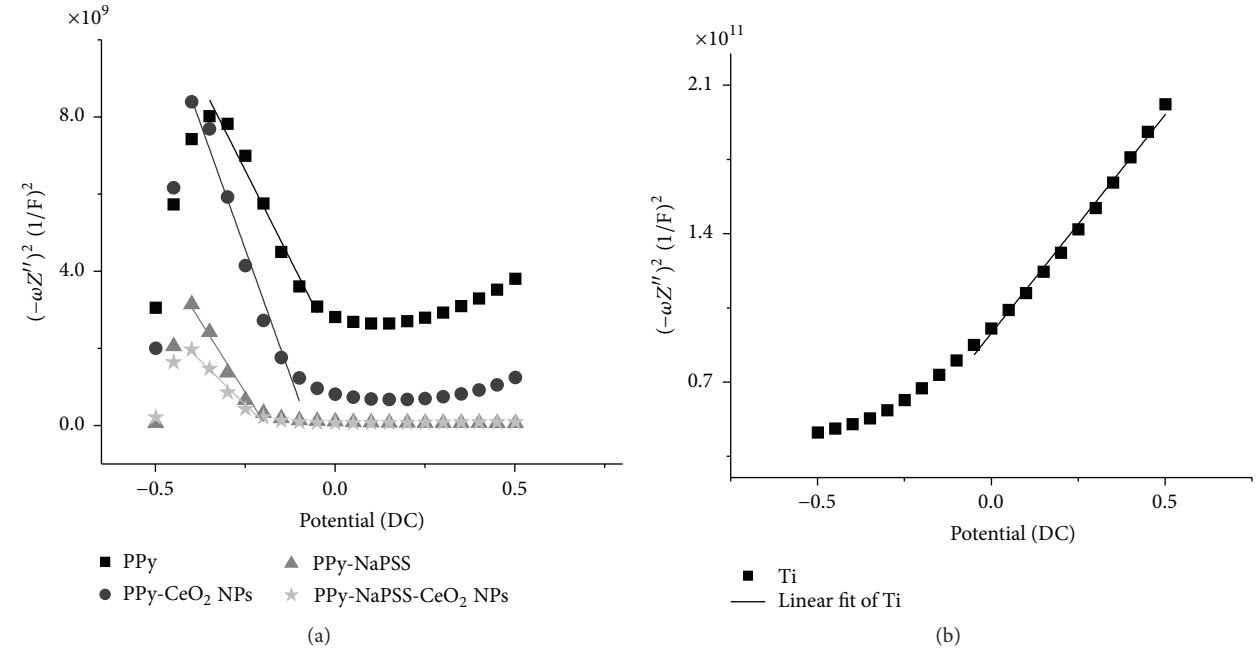

Figure 8: Mott-Schottky diagrams for (a) Ti/PPy films and (b) uncoated titanium.

Table 2: The contact angle measurements and standard deviations for PPy-nanocomposite films.

Coating film	Contact angle, degrees	SD
Ti/PPy	86.61	±2.29
Ti/PPy-NaPSS	52.15	±2.53
Ti/PPy-CeO_2 NPs	78.64	±1.88
Ti/PPy-NaPSS-CeO_2 NPs	53.88	±1.33

3.4. Electrochemical Characterization of PPy-Nanocomposite Films in Buffer Solution

3.4.1. Mott-Schottky Analysis. In order to emphasize the changes in polymer films during CeO_2 and/or surfactant embedding in the structure of PPy, the characterizations were supplemented with Mott-Schottky analysis. This technique based on capacitance versus potential measurements is a common *in situ* method for investigation of polymeric films semiconductor properties. Figure 8 presents the experimental data and the fit of linear domains of Mott-Schottky diagrams for all anodized samples. A positive slope can be observed for uncoated titanium, typical for *n*-type semiconductor, and negative slopes for polypyrrole coated titanium, typical for *p*-type semiconductor.

The flat band potential (E_{fb}) and charge carrier density (N_d) data calculated from Mott-Schottky diagrams show significant changes in the semiconductor properties of the polypyrrole films during CeO_2 NPs incorporation, Table 3.

After insertion of CeO_2 in/onto PPy film, E_{fb} is shifted in negative direction with about 180 mV, confirming that CeO_2 NPs are positively charged in acid aqueous polymerization solution. N_d of PPy film decreases in the presence of CeO_2 NPs from $7.63 \cdot 10^{18}\ m^{-3}$ to $5.39 \cdot 10^{18}\ m^{-3}$, sustaining the negative influence of ceria nanoparticles over PPy doping, highlighted by EDX analysis and electrochemical polymerization process.

CeO_2 nanoparticles insertion performed in the presence of surfactant has not caused a shifting of E_{fb}, −192 mV for PPy-NaPSS, and −191 mV for PPy-NaPSS-CeO_2. Moreover, the presence of anionic surfactant in the polypyrrole film is clearly evidenced by a shifting of E_{fb} in cathodic direction, with about 300 mV and an increase of the charge carrier density of PPy film from $7.63 \cdot 10^{18}\ m^{-3}$ to $9.52 \cdot 10^{18}\ m^{-3}$. Furthermore, the increase of E_{fb} of PPy-NaPSS film after CeO_2 NPs insertion, from $9.52 \cdot 10^{18}\ m^{-3}$ to $1.548 \cdot 10^{19}\ m^{-3}$, shows that, in this situation, the negative effect of ceria nanoparticles on the doping process is not observed in the presence of surfactant. Thus, the influence of surfactant is prevalent on the doping process due to the presence of the adsorbed surfactant cage around ceria nanoparticles.

3.4.2. Electrochemical Impedance Spectroscopy. Electrochemical impedance spectroscopy performed at open circuit potential in buffer solution was discussed in terms of Nyquist plots (Figure 9).

The equivalent electric circuits used to fit the EIS data with Nova software are represented in Figure 10. For PPy and PPy-CeO_2 NPs films, a two-time constant circuit was used (Figure 10(a)), where R_s is solution resistance, R_{ct1} is the resistance responsible for the ion transfer through polymeric film, connected in parallel with a constant phase element CPE_1, and n is the phase change values. R_{ct2} is the resistance responsible for the electron transfer and CPE_2 is the second constant phase element for electric double layer. Another constant phase element CPE_3 was introduced for

Table 3: Charge carrier density (N_d) and flat band potential (E_{fb}) from Mott-Schottky diagrams.

Electrical parameters	PPy	PPy-CeO_2 NPs	PPy-NaPSS	PPy-NaPSS-CeO_2 NPs
E_{fb} (V)	0.108	−0.075	−0.192	−0.191
N_d (m^{-3})	$7.630 \cdot 10^{18}$	$5.395 \cdot 10^{18}$	$0.952 \cdot 10^{19}$	$1.548 \cdot 10^{19}$

Table 4: Electric parameters from fitting experimental EIS data.

Parameters	Polymeric-nanocomposite films			
	PPy	PPy-CeO_2 NPs	PPy-NaPSS	PPy-NaPSS-CeO_2 NPs
R_s ($\Omega\,cm^2$)	119	25.1	117	160
R_{ct1} ($\Omega\,cm^2$)	83.2	51.5	$6.810 \cdot 10^{+3}$	$4.370 \cdot 10^{+3}$
CPE_1 ($\Omega^{-1}\,cm^{-2}\,s^n$)	$3.96 \cdot 10^{-3}$	$7.99 \cdot 10^{-6}$	$1.860 \cdot 10^{-3}$	$1.370 \cdot 10^{-3}$
n_1	0.773	0.360	0.868	0.785
R_{ct2} ($\Omega\,cm^2$)	56	117	—	—
CPE_2 ($\Omega^{-1}\,cm^{-2}\,s^n$)	$9.750 \cdot 10^{-6}$	$4.050 \cdot 10^{-3}$	—	—
n_2	0.342	0.790	—	—
CPE_3 ($\Omega^{-1}\,cm^{-2}\,s^n$)	$5.570 \cdot 10^{-3}$	$5.12 \cdot 10^{-3}$	—	—
n_3	0.963	0.976	—	—

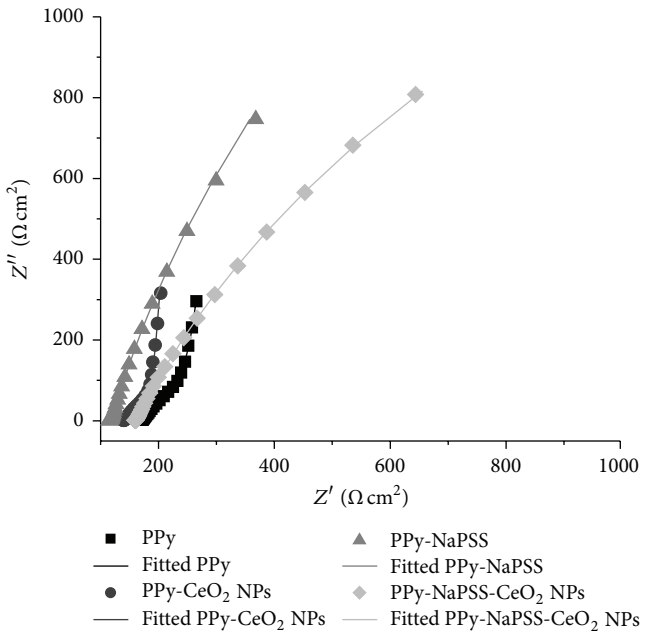

Figure 9: Nyquist spectra for PPy-nanocomposite films/Ti in buffer solution.

lower frequency corresponding to capacitive behaviour of these films [40].

On the other hand, for more compact PPy-nanocomposite films, PPy-NaPSS and PPy-NaPSS-CeO_2 NPs, the EIS data were fitted with an equivalent electric circuit with one-time constant (Figure 10(b)), where R_s is solution resistance, R_{ct1} is charge transfer resistance, and CPE_1 is constant phase element.

Electric parameters obtained from fitted experimental EIS data with proposed equivalent circuits are presented in Table 4.

The presence of the cationic oxide CeO_2 NPs in polymerization solution is reflected by the values of the electron transfer resistance (R_{ct2}). For PPy-CeO_2 NPs film, R_{ct2} is higher ($117\,\Omega\,cm^2$) comparing with that of PPy film ($56\,\Omega\,cm^2$). This observation is in accordance with charge carrier density (N_d) values obtained from Mott-Schottky analysis which are superior for PPy film than PPy-CeO_2NPs. However, R_{ct1}, associated with ion transfer resistance, decreases when CeO_2 NPs were added in the polymeric film, probably due to a presumed increase in ionic film permeability, as was reported in literature [37].

Also, in NaPSS presence the charge transfer resistance increased with one order of magnitude compared to those of polymeric films without surfactant, which could suggests that the resulted PPy-NaPSS films are more compact and stable. On the other hand, N_d values obtained from Mott-Schottky analysis indicated an increase in PPy doping process in the presence of surfactant. Thus, although PPy film which resulted in the presence of surfactant should be more conductive, the resistance values are higher. This behaviour can be explained on the base of parallel adsorption processes of PSS^- on titanium surface at the beginning of anodic polymerization that leads to a possible partial passivation of the substrate.

The embedding of CeO_2 NPs into PPy-NaPSS-CeO_2 NPs film shows a decreasing of charge transfer resistance, from $6.81\,k\Omega{\cdot}cm^2$ to $4.37\,k\Omega{\cdot}cm^2$, probably due to the similar processes presented above. n value of constant phase element is also slightly reduced from 0.86 to 0.78, sustaining a reduction in capacitive behaviour of the polypyrrole film, due to ionic permeation.

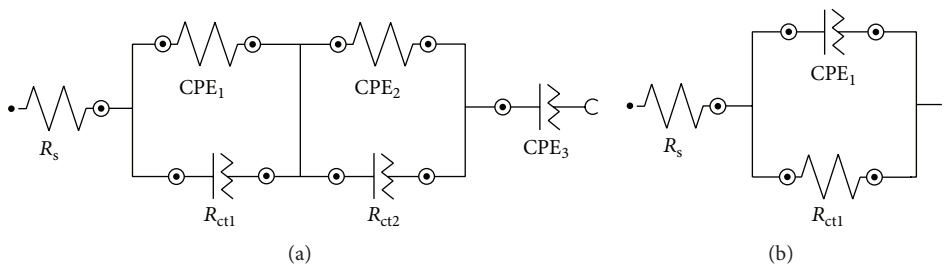

Figure 10: The equivalent circuits used to fit EIS data for (a) PPy and PPy-CeO_2 NPs films and (b) PPy-NaPSS and PPy-NaPSS-CeO_2 NPs films.

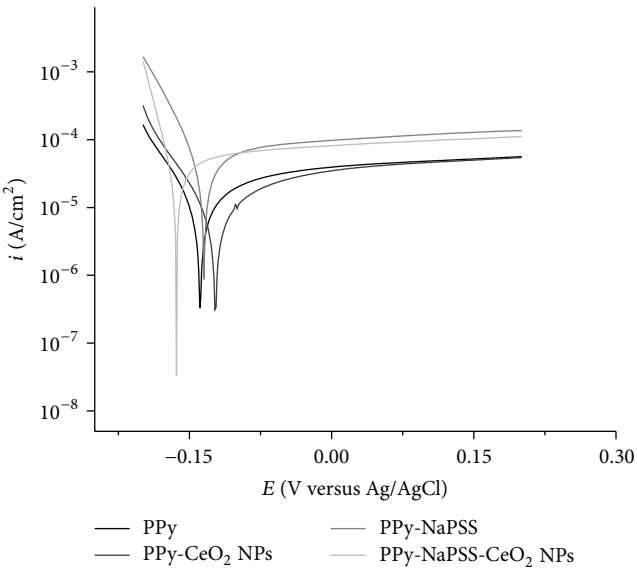

Figure 11: Tafel diagrams for PPy-nanocomposite films on Ti in buffer solution.

3.4.3. Tafel Diagrams. Figure 11 shows the set of polarization curves recorded for PPy-nanocomposite films in buffer solution.

The electrochemical parameters computed with Nova software are presented in Table 5.

The polarization resistance (R_p) values obtained from Tafel analysis performed in d.c. current depend on many surface features, such as film conductivity associated with the doping process, film permeability, substrate passivation connected with surfactant adsorption, and titanium oxide formation.

R_p values from Tafel plots for PPy and PPy-CeO_2 NPs films are different than the R_{ct} values obtained from EIS (performed in a.c. current) with about one order of magnitude. These different results obtained by different techniques could be due to the effect of electrical imposed perturbations on the coating properties. The EIS analysis is performed at free potential with small perturbation amplitude of 10 mV and the film properties are not importantly affected. On the contrary, Tafel analysis is performed in ±200 mV perturbation, stimulating reduction/oxidation processes (undoping/doping) of the polypyrrole film which involve insertion/repulsion of anions and cations into/through the polymeric film, as represented in (3) and (4) [40]. One has

$$\mathrm{PPy} + n\mathrm{A}^- \xrightarrow{\text{oxidation}} \left[(\mathrm{PPy})^{n+}(\mathrm{A}^-)_n\right] + ne^- \quad (3)$$

$$\left[(\mathrm{PPy})^{n+}(\mathrm{A}^-)_n\right] + n\mathrm{C}^+ + ne^- \xrightarrow{\text{reduction}} \left[(\mathrm{PPy})(\mathrm{A}^-)_n(\mathrm{C}^+)_n\right] \quad (4)$$

These insertion/repulsion processes lead to increase of PPy film permeability and the electrolyte can reach more easily to the surface of titanium substrate, promoting the resistive TiO_2 oxide layer formation between PPy film and Ti. For PPy-NaPSS and PPy-NaPSS-CeO_2 NPs films, R_p values obtained from Tafel plots are in a good correlation with those obtained from EIS data, sustaining once again the stability and the less permeability of PPy-NaPSS films conferred by the presence of surfactant. The PSS^- mobility during potential perturbation is reduced comparing with oxalate anion. Thus, the film remains more compact avoiding the electrolyte insertion.

3.5. Antibacterial Activity. In Figure 12 the influence of CeO_2 NPs bonded in PPy matrix on antibacterial activity of polymeric film was represented.

The presence of uniform spreading CeO_2 NPs agglomerates onto polymeric matrix (PPy-CeO_2) improves the antibacterial activity of the polymeric film, being in accordance with the literature data which specified that the nanoparticles of CeO_2 have a good antibacterial effect on *Escherichia coli* [44].

PPy-NaPSS-CeO_2 NPs film has a slightly lower antibacterial activity than PPy-CeO_2 NPs film. The different doping process in the presence of NaPSS and the better embedding of negatively charged CeO_2 NPs lead to a small amount of CeO_2 NPs on the polymer surface.

Thus, the role of the surfactant becomes determinant during polymerization and the interaction between CeO_2 NPs and PPy films has a strong influence on antibacterial activity. If the nanoparticles are on the polymer surface, the antibacterial effect is improved but if nanoparticles are

Table 5: Electrochemical parameters from Tafel diagrams.

Electrochemical parameters	PPy	PPy-CeO_2 NPs	PPy-NaPSS	PPy-NaPSS-CeO_2 NPs
E_{cor} (mV)	−138	−125	−135	−167
i_{cor} (μA/cm^2)	19.390	12.321	53.300	22.268
v_{cor} (mm/year)	0.169	0.107	0.464	0.194
R_p (kΩ)	4.617	6.206	1.083	1.060

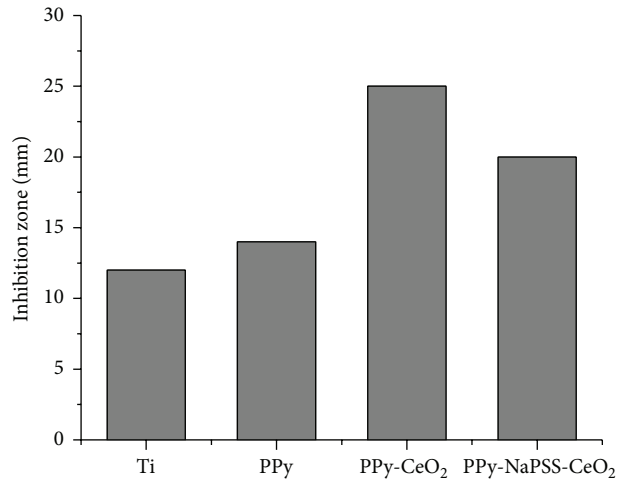

Figure 12: Antibacterial activity of PPy-nanocomposite films on *Escherichia coli*.

preponderantly embedded into PPy film, the antibacterial activity is slightly decreased.

The results obtained from antibacterial activity of PPy-nanocomposite films on *Escherichia coli* confirm and sustain the observations arising out from the surface and electrochemical analysis regarding CeO_2 NPs bonding into/onto polymeric matrix.

4. Conclusions

CeO_2 nanoparticles with dimension of tens nanometers were synthesized by a coprecipitation method. The influence of NaPSS surfactant on the embedded CeO_2 NPs in polypyrrole films was investigated. CeO_2 nanoparticles with dimension of tens nanometers were synthesized by a coprecipitation method and embedded in polypyrrole films in presence of NaPSS surfactant.

From surface and electrochemical characterization it was highlighted that NaPSS surfactant and CeO_2 NPs play an important role in PPy doping process. NaPSS presence improves CeO_2 NPs embedding into PPy matrix. The adsorption of PSS^- anions on the nanoparticles surface leads to negatively charged CeO_2 NPs and improves the electrostatic interactions with cationic PPy^+ matrix (doping).

In the presence of surfactant CeO_2 NPs are preferentially embedded in the polymeric film while, without surfactant, the ceria nanoparticles are quasiuniformly spread as agglomerates onto polymeric films.

This different distribution of ceria nanoparticles into/onto polypyrrole influences the film stability and even its possible applications.

Competing Interests

The authors declare that they have no competing interests.

Acknowledgments

This work was supported by a project of CNCS-UEFISCDI, PN2-253/2014-NANOCOAT. The authors wish to thank Ms. Cristina Nicolescu for XRD analysis and Ms. Camelia Ungureanu for antibacterial activity analysis.

References

[1] J. L. Chen, C. Chen, Z. Y. Chen, J. Y. Chen, Q. L. Li, and N. Huang, "Collagen/heparin coating on titanium surface improves the biocompatibility of titanium applied as a blood-contacting biomaterial," *Journal of Biomedical Materials Research Part A*, vol. 95, no. 2, pp. 341–349, 2010.

[2] M. Geetha, A. K. Singh, R. Asokamani, and A. K. Gogia, "Ti based biomaterials, the ultimate choice for orthopaedic implants-a review," *Progress in Materials Science*, vol. 54, no. 3, pp. 397–425, 2009.

[3] W. Ma, S.-H. Wang, G.-F. Wu et al., "Preparation and *in vitro* biocompatibility of hybrid oxide layer on titanium surface," *Surface and Coatings Technology*, vol. 205, no. 6, pp. 1736–1742, 2010.

[4] S. Mei, H. Wang, W. Wang et al., "Antibacterial effects and biocompatibility of titanium surfaces with graded silver incorporation in titania nanotubes," *Biomaterials*, vol. 35, no. 14, pp. 4255–4265, 2014.

[5] Y.-H. Lee, G. Bhattarai, S. Aryal et al., "Modified titanium surface with gelatin nano gold composite increases osteoblast cell biocompatibility," *Applied Surface Science*, vol. 256, no. 20, pp. 5882–5887, 2010.

[6] K. Gulati, S. Ramakrishnan, M. S. Aw, G. J. Atkins, D. M. Findlay, and D. Losic, "Biocompatible polymer coating of titania nanotube arrays for improved drug elution and osteoblast adhesion," *Acta Biomaterialia*, vol. 8, no. 1, pp. 449–456, 2012.

[7] S. K. Mishra and S. Kannan, "Development, mechanical evaluation and surface characteristics of chitosan/polyvinyl alcohol based polymer composite coatings on titanium metal," *Journal of the Mechanical Behavior of Biomedical Materials*, vol. 40, pp. 314–324, 2014.

[8] S. K. Mishra, J. M. F. Ferreira, and S. Kannan, "Mechanically stable antimicrobial chitosan-PVA-silver nanocomposite coatings deposited on titanium implants," *Carbohydrate Polymers*, vol. 121, pp. 37–48, 2015.

[9] K. Ishihara and J. Chol, "Biocompatible polymer assembly on metal surfaces," *Metals for Biomedical Devices*, pp. 283–302, 2010.

[10] H. Chen, L. Yuan, W. Song, Z. Wu, and D. Li, "Biocompatible polymer materials: role of protein-surface interactions," *Progress in Polymer Science*, vol. 33, no. 11, pp. 1059–1087, 2008.

[11] G. Hélary, F. Noirclère, J. Mayingi, and V. Migonney, "A new approach to graft bioactive polymer on titanium implants: improvement of MG 63 cell differentiation onto this coating," *Acta Biomaterialia*, vol. 5, no. 1, pp. 124–133, 2009.

[12] G. Tan, L. Zhou, C. Ning et al., "Biomimetically-mineralized composite coatings on titanium functionalized with gelatin methacrylate hydrogels," *Applied Surface Science*, vol. 279, pp. 293–299, 2013.

[13] A. de Leon and R. C. Advincula, "Conducting polymers with superhydrophobic effects as anticorrosion coating," in *Intelligent Coatings for Corrosion Control*, A. Tiwari, L. Hihara, and J. Rawlins, Eds., pp. 409–430, 2015.

[14] P. Zarras and J. D. Stenger-Smith, "Electro-active polymer (EAP) coatings for corrosion protection of metals," in *Handbook of Smart Coatings for Materials Protection*, A. S. H. Makhlouf, Ed., pp. 328–369, Woodhead, Cambridge, UK, 2014.

[15] D. D. Ateh, P. Vadgama, and H. A. Navsaria, "Culture of human keratinocytes on polypyrrole-based conducting polymers," *Tissue Engineering*, vol. 12, no. 4, pp. 645–655, 2006.

[16] Y. Li, K. G. Neoh, L. Cen, and E. T. Kang, "Porous and electrically conductive polypyrrole- Poly (vinyl alcohol) composite and its applications as a biomaterial," *Langmuir*, vol. 21, no. 23, pp. 10702–10709, 2005.

[17] G. M. Spinks, V. Mottaghitalab, M. Bahrami-Samani, P. G. Whitten, and G. G. Wallace, "Carbon-nanotube-reinforced polyaniline fibers for high-strength artificial muscles," *Advanced Materials*, vol. 18, no. 5, pp. 637–640, 2006.

[18] E. De Giglio, M. R. Guascito, L. Sabbatini, and G. Zambonin, "Electropolymerization of pyrrole on titanium substrates for the future development of new biocompatible surfaces," *Biomaterials*, vol. 22, no. 19, pp. 2609–2616, 2001.

[19] K. Idla, O. Inganäs, and M. Strandberg, "Good adhesion between chemically oxidised titanium and electrochemically deposited polypyrrole," *Electrochimica Acta*, vol. 45, no. 13, pp. 2121–2130, 2000.

[20] X. Wang, X. Gu, C. Yuan et al., "Evaluation of biocompatibility of polypyrrole *in vitro* and *in vivo*," *Journal of Biomedical Materials Research—Part A*, vol. 68, no. 3, pp. 411–422, 2004.

[21] S. T. Earley, D. P. Dowling, J. P. Lowry, and C. B. Breslin, "Formation of adherent polypyrrole coatings on Ti and Ti-6Al-4V alloy," *Synthetic Metals*, vol. 148, no. 2, pp. 111–118, 2005.

[22] Z. Weiss, D. Mandler, G. Shustak, and A. J. Domb, "Pyrrole derivatives for electrochemical coating of metallic medical devices," *Journal of Polymer Science Part A: Polymer Chemistry*, vol. 42, no. 7, pp. 1658–1667, 2004.

[23] M. Mîndroiu, C. Ungureanu, R. Ion, and C. Pîrvu, "The effect of deposition electrolyte on polypyrrole surface interaction with biological environment," *Applied Surface Science*, vol. 276, pp. 401–410, 2013.

[24] S. M. Dizaj, F. Lotfipour, M. Barzegar-Jalali, M. H. Zarrintan, and K. Adibkia, "Antimicrobial activity of the metals and metal oxide nanoparticles," *Materials Science and Engineering C*, vol. 44, pp. 278–284, 2014.

[25] R. Gokulakrishnan, S. Ravikumar, and J. A. Raj, "*In vitro* antibacterial potential of metal oxide nanoparticles against antibiotic resistant bacterial pathogens," *Asian Pacific Journal of Tropical Disease*, vol. 2, no. 5, pp. 411–413, 2012.

[26] M. Moritz and M. Geszke-Moritz, "The newest achievements in synthesis, immobilization and practical applications of antibacterial nanoparticles," *Chemical Engineering Journal*, vol. 228, pp. 596–613, 2013.

[27] A. S. Karakoti, N. A. Monteiro-Riviere, R. Aggarwal et al., "Nanoceria as antioxidant: synthesis and biomedical applications," *The Journal of The Minerals, Metals & Materials Society*, vol. 60, no. 3, pp. 33–37, 2008.

[28] V. Shah, S. Shah, H. Shah et al., "Antibacterial activity of polymer coated cerium oxide nanoparticles," *PLoS ONE*, vol. 7, article e47827, 2012.

[29] C. H. Baker, "Harnessing cerium oxide nanoparticles to protect normal tissue from radiation damage," *Translational Cancer Research*, vol. 2, pp. 343–358, 2013.

[30] F. Liu, Y. Yuan, L. Li et al., "Synthesis of polypyrrole nanocomposites decorated with silver nanoparticles with electrocatalysis and antibacterial property," *Composites Part B: Engineering*, vol. 69, pp. 232–236, 2014.

[31] M. B. González, L. I. Brugnoni, M. E. Vela, and S. B. Saidman, "Silver deposition on polypyrrole films electrosynthesized in salicylate solutions," *Electrochimica Acta*, vol. 102, pp. 66–71, 2013.

[32] E. N. Zare, M. M. Lakouraj, and M. Mohseni, "Biodegradable polypyrrole/dextrin conductive nanocomposite: synthesis, characterization, antioxidant and antibacterial activity," *Synthetic Metals*, vol. 187, no. 1, pp. 9–16, 2014.

[33] M. Cabuk, Y. Alan, M. Yavuz, and H. I. Unal, "Synthesis, characterization and antimicrobial activity of biodegradable conducting polypyrrole-graft-chitosan copolymer," *Applied Surface Science*, vol. 318, pp. 168–175, 2014.

[34] C. Ungureanu, C. Pirvu, M. Mindroiu, and I. Demetrescu, "Antibacterial polymeric coating based on polypyrrole and polyethylene glycol on a new alloy TiAlZr," *Progress in Organic Coatings*, vol. 75, no. 4, pp. 349–355, 2012.

[35] C. Ungureanu, S. Popescu, G. Purcel et al., "Improved antibacterial behavior of titanium surface with torularhodin-polypyrrole film," *Materials Science and Engineering C*, vol. 42, pp. 726–733, 2014.

[36] K.-Q. Liu, C.-X. Kuang, M.-Q. Zhong, Y.-Q. Shi, and F. Chen, "Synthesis, characterization and UV-shielding property of polystyrene-embedded CeO_2 nanoparticles," *Optical Materials*, vol. 35, no. 12, pp. 2710–2715, 2013.

[37] C. Benmouhoub, J. Agrisuelas, N. Benbrahim et al., "Influence of the incorporation of CeO_2 nanoparticles on the ion exchange behavior of dodecylsulfate doped polypyrrole films: Ac-electrogravimetry investigations," *Electrochimica Acta*, vol. 145, pp. 270–280, 2014.

[38] C. Pirvu, M. Mindroiu, S. Popescu, and I. Demetrescu, "Electrodeposition of polypyrrole/poly(Styrene Sulphonate) composite coatings on Ti6Al7Nb alloy," *Molecular Crystals and Liquid Crystals*, vol. 521, pp. 126–139, 2010.

[39] M. Mindroiu, R. Ion, C. Pirvu, and A. Cimpean, "Surfactant-dependent macrophage response to polypyrrole-based coatings electrodeposited on Ti_6Al_7Nb alloy," *Materials Science and Engineering C*, vol. 33, no. 6, pp. 3353–3361, 2013.

[40] C. Pirvu, C. C. Manole, A. B. Stoian, and I. Demetrescu, "Understanding of electrochemical and structural changes of polypyrrole/polyethylene glycol composite films in aqueous solution," *Electrochimica Acta*, vol. 56, no. 27, pp. 9893–9903, 2011.

[41] J. H. Jorgensen and J. D. Turnidge, *Susceptibility Test Methods: Dilution and Disk Diffusion Methods*, ASM Press, 2015.

[42] R. Bouldin, S. Ravichandran, A. Kokil et al., "Synthesis of polypyrrole with fewer structural defects using enzyme catalysis," *Synthetic Metals*, vol. 161, no. 15-16, pp. 1611–1617, 2011.

[43] A. Sehgal, Y. Lalatonne, J.-F. Berret, and M. Morvan, "Precipitation-redispersion of cerium oxide nanoparticles with poly (acrylic acid): toward stable dispersions," *Langmuir*, vol. 21, no. 20, pp. 9359–9364, 2005.

[44] Y. Kuang, X. He, Z. Zhang et al., "Comparison study on the antibacterial activity of nano-or bulk-cerium oxide," *Journal of Nanoscience and Nanotechnology*, vol. 11, no. 5, pp. 4103–4108, 2011.